Ultrasensitive Strain Modulation of Terahertz Magnons at a Magnetic Phase Transition

Lichen Wang[1,*] Sajna Hameed[1] Yiran Liu[1] Manuel Knauft[1] Kazuki Higuchi,[1] Maximilian Krautloher[1] Sonia Francoual[2] Giniyat Khaliullin[1] Huimei Liu[1,3,4,†] Matteo Minola,[1,‡] and Bernhard Keimer[1,§]

[1]*Max Planck Institute for Solid State Research, Heisenbergstrasse 1, D-70569 Stuttgart, Germany*

[2]*Deutsches Elektronen-Synchrotron DESY, Notkestrasse 85, D-22607 Hamburg, Germany*

[3]*National Laboratory of Solid State Microstructures and School of Physics, Nanjing University, Nanjing 210093, China*

[4]*Collaborative Innovation Center of Advanced Microstructures, Nanjing University, Nanjing 210093, China*

(Received 19 May 2026; accepted 26 October 2026; published 16 November 2026)

Motivated by the prospect of strain control of terahertz (THz) magnons, we have used resonant x-ray diffraction and Raman scattering to investigate the magnetic ground state and excitations of the layered Mott insulator Ca_2RuO_4 under uniaxial strain. We discovered a strain-induced phase transition between two antiferromagnetic states that differ in the sign of the interlayer exchange interaction. Although this interaction is weak and partially frustrated, the corresponding magnon energies of the two states differ by more than 10% (∼0.3 THz). Our theoretical analysis explains this surprising observation by tracing the origin of both the sign reversal of the interlayer coupling and the magnon energy to the spin-orbital composition of the Ru valence electrons. The extreme strain sensitivity of the THz magnon energy near a magnetic phase transition opens up pathways toward a new generation of "transition-edge" magnonic devices.

DOI: 10.1103/wk6v-1x5s

The controlled manipulation of collective spin excitations (magnons) in antiferromagnets is of intense current interest, driven by the prospect of exploring ultrafast terahertz (THz) spin dynamics free from the parasitic stray fields of ferromagnets [1]. While the generation and detection of these high-frequency magnons have seen rapid progress, effectively tuning their energy spectra remains a fundamental challenge. Current approaches to achieve such modulation include electric-field control of "electro-magnons" in multiferroics [1] and uniaxial strain tuning of THz magnons in antiferromagnets [2].

Here we show that the sensitivity of these modulations can be greatly enhanced in the vicinity of strain-induced magnetic phase transitions. Such transitions have recently been reported in various quasi-two-dimensional (quasi-2D) magnets under different strain variants. Examples include uniaxial strain in the van der Waals magnet CrSBr [3] and the triangular antiferromagnet $PdCrO_2$ [4], as well as biaxial [5] or shear [6] strain in the square-lattice antiferromagnet Sr_2IrO_4. In these systems, the phase transition separates different stacking patterns of magnetic layers where intralayer exchange interactions greatly exceed the interlayer coupling. Since the mechanism involves strain modulation of the weak interlayer exchange, the resulting magnon energy difference between the two states is expected to be small. In line with this expectation, recent experiments on CrSBr field-effect devices have detected magnon energy shifts in the GHz regime [7].

We have performed resonant x-ray diffraction (RXD) and Raman scattering experiments on the quasi-2D square-lattice antiferromagnet Ca_2RuO_4 with Néel temperature $T_N = 113$ K [8]. Its Ru ions host spin-orbit entangled pseudospins [9] with interlayer exchange that is nearly frustrated due to the body-centered stacking [Fig. 2(c)]; thus, the net coupling between the layers is only stabilized by the small orthorhombic distortion. While ambient Ca_2RuO_4 exhibits an "A-centered" antiferromagnetic (AFM) structure, a "B-centered" state with reversed interlayer coupling has been uncovered in pressurized, doped or off-stoichiometric compounds featuring subtly different lattice structures [8,10–15]. Our experiments demonstrate that this A-centered to B-centered transition can also be driven in pure Ca_2RuO_4 by ∼0.15% uniaxial strain. Surprisingly, this transition is associated with an abrupt, reversible jump of the zone-center magnon energy from ∼3.0 to 3.3 THz—orders of magnitude larger than the expected influence of the weak interlayer interactions ($J_c \sim 4 \times 10^{-3}$ THz [16,17]). We present a quantitative

*Contact author: lichen.wang@fkf.mpg.de

†Contact author: huimeiliu@nju.edu.cn

‡Contact author: m.minola@fkf.mpg.de

§Contact author: b.keimer@fkf.mpg.de

Published by the American Physical Society under the terms of the Creative Commons Attribution 4.0 International license. Further distribution of this work must maintain attribution to the author(s) and the published article's title, journal citation, and DOI. Open access publication funded by the Max Planck Society.

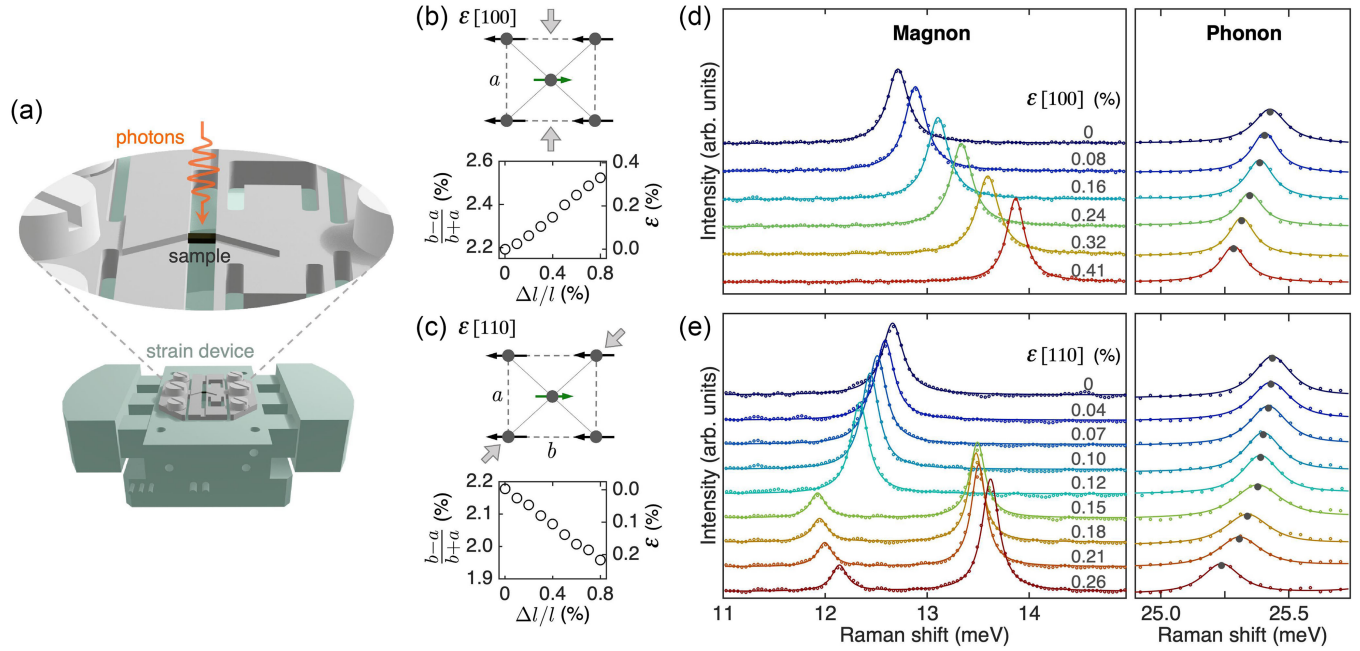


FIG. 1. (a) Schematic of the uniaxial strain setup. (b) Top: schematic of strain application along the [1 0 0] direction. Black circles represent Ru ions, where black and green arrows indicate antiparallel pseudospins along the b axis. Bottom: lattice orthorhombicity $(b-a)/(b+a)$ and effective strain ε under compression along the [1 0 0] direction, where $\Delta l/l$ is the normalized piezoelectric displacement. (c) Same as (b) but for strain along the [1 1 0] direction. (d),(e) Raman spectra at $T = 25$ K under varying compressive strain along the [1 0 0] and [1 1 0] directions, respectively. The data display magnon spectra in the B_{1g} channel and phonon spectra in the A_g channel, with black dots marking phonon energies.

theory explaining both the energy jump and the sign reversal of the interlayer coupling in terms of strain-induced modulation of the spin-orbit admixture of the Ru pseudospins. The discovery of a large magnon energy difference between nearly identical magnetic ground states separated by a sharp phase transition opens avenues for magnonic devices with piezo-tunable interface transparency. The critical strain could be tuned toward zero through lattice engineering, allowing a magnonic switch to operate at lower applied strain.

Experiment—The strain setup for Raman and x-ray scattering is illustrated in Fig. 1(a) (see experimental details in Supplemental Material [18]). This system has been successfully used in several spectroscopic studies of correlated electron systems [2,21,22]. Compressive strain was applied along two in-plane directions: [1 0 0] (next-nearest-neighbor Ru-Ru bonds) and [1 1 0] (nearest-neighbor Ru-Ru bonds), as shown in Figs. 1(b) and 1(c), respectively. The in-plane strain directly modifies the lattice orthorhombicity, defined as $(b-a)/(b+a)$, where a and b are the lattice constants with $b > a$. The orthorhombicity exhibits nearly linear but opposite responses to the two compression directions [Figs. 1(b) and 1(c)]. We define an effective strain $\varepsilon = |(b-a)/(b+a) - \varepsilon_0|$ to quantify the absolute change from the intrinsic zero-strain value ε_0, where $\varepsilon > 0$ denotes compression.

Figures 1(d) and 1(e) present the Raman spectra of magnons and phonons under varying strain. In the AFM state ($T = 25$ K), unstrained Ca_2RuO_4 exhibits a sharp and intense magnon feature at 12.7 meV (3.07 THz) in the B_{1g} channel [23], consistent with the magnon gap measured by inelastic neutron scattering [24]. Compression along the shorter a axis ([1 0 0] direction) enhances the orthorhombicity [Fig. 1(b)], increasing the magnetic anisotropy via pseudospin-lattice coupling [25] and driving a clear blue shift of the magnon peak [Fig. 1(d)]. Under this applied strain, both the magnon and phonon peaks exhibit nearly linear responses [Figs. 1(d) and 3].

We now focus on a remarkable anomaly in the magnon spectrum under compressive strain along the [1 1 0] direction [Fig. 1(e)]. At a critical strain $\varepsilon_c \sim 0.15\%$, the B_{1g} magnon splits into two components, whose combined spectral weight matches that of the original magnon (Fig. S7 [18]). The dominant peak shifts abruptly by $\sim$0.3 THz ($> 10\%$) above the pretransition energy, while the minor feature remains slightly below it. Upon warming, both modes rapidly broaden and weaken (Fig. S4 [18]), exhibiting a temperature dependence analogous to the zero-strain magnon rather than phonons [23], thereby confirming their magnetic origin. The strain-driven magnon anomaly signals a fully reproducible magnetic phase transition near ε_c (Fig. S7 [18]), as further corroborated by our RXD measurements.

Figure 1(e) also reveals a sharp contrast in the strain dependence of the magnon energy across ε_c. At low strain,

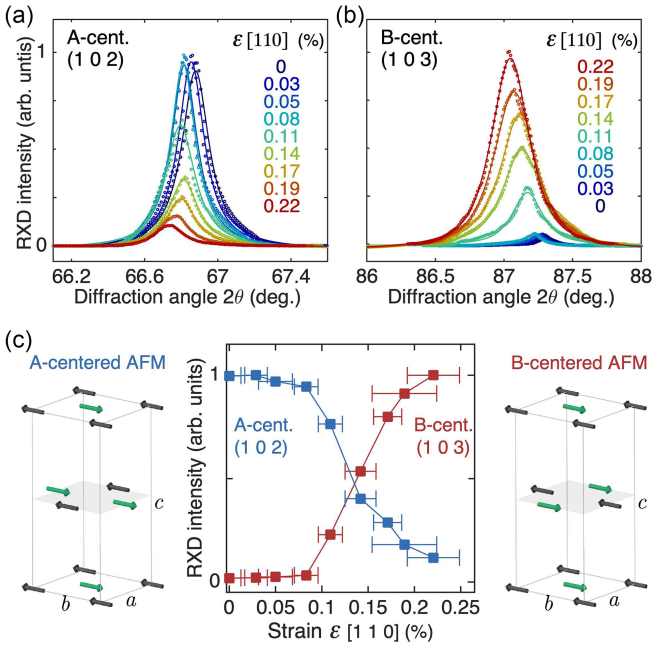


FIG. 2. (a),(b) Magnetic reflections of the A- and B-centered AFM orders measured via RXD at $T = 20$ K under compressive strain along the [1 1 0] direction. The A- and B-centered phases are characterized by ($h + l$ odd, $k + l$ even) and ($h + l$ even, $k + l$ odd) reflections, respectively. (c) Strain dependence of integrated intensities for the A-centered (blue) and B-centered (red) reflections, normalized to their respective maxima. Error bars represent strain uncertainties derived from simultaneous lattice constant measurements [18]. Side panels: schematics of the A- and B-centered magnetic structures; arrows denote Ru pseudospins. In both structures, the ordered moments are slightly canted (not shown here) away from the b axis [26,27]; the resulting canted moments are stacked antiferromagnetically between adjacent layers in the A-centered phase but ferromagnetically in the B-centered phase [8].

the magnon peak exhibits a nearly linear red shift, whereas above ε_c the energies of both magnon features increase nonlinearly with strain. While the reduced orthorhombicity [Fig. 1(c)] explains the initial red shift below ε_c, it cannot account for the nonlinear energy increase above the transition. This points to underlying mechanisms beyond mere orthorhombicity changes, as addressed in the theoretical analysis below.

We further observe that the contrasting effects of compression along the [1 0 0] and [1 1 0] directions on the lattice orthorhombicity [Figs. 1(b) and 1(c), respectively] are reflected in the lattice dynamics: most phonon modes shift in opposite directions (Fig. S3 [18]). An exception is the A_g phonon at 25.4 meV, which softens under both in-plane compression directions [Figs. 1(d) and 1(e)], indicating that its eigenmode involves atomic vibrations along the expanding c axis. Notably, the strain dependence of the mode frequency exhibits a kink at ε_c [Figs. 1(e) and S6(b) [18]]. Similar anomalies are also observed in other phonon modes, collectively suggesting structural modifications associated with the magnetic phase transition. However, the absence of new phonon modes implies that the lattice symmetry remains unchanged.

As shown in Fig. 2, RXD measurements at the Ru L_3 edge track the strain-driven magnetic transition on the same sample used for Raman spectroscopy. Figures 2(a) and 2(b) show the evolution of (1 0 2) and (1 0 3) Bragg reflections, respectively, which represent the A-centered and B-centered AFM structures, respectively [Fig. 2(c)]. Their magnetic space groups are $Pbca$ and $Pbc'a'$, corresponding to magnetic point groups mmm and $mm'm'$, respectively [26,27]. These two phases possess identical in-plane spin order but opposite interlayer coupling signs [28].

With increasing compressive strain along the [1 1 0] direction, the (1 0 2) reflection intensity is suppressed as the (1 0 3) reflection emerges from the background, indicating an A-centered to B-centered phase transition at $\varepsilon_c \sim 0.15\%$. This transition is completely reversible upon strain release (Fig. S8 [18]). While the B-centered phase is typically stabilized by doping or pressure [8,10–15], our results demonstrate its realization via modest uniaxial strain. Furthermore, the strain-stabilized B-centered phase exhibits a higher Néel temperature ($T_N \sim 135$ K, Fig. S9 [18]) than the A-centered phase ($T_N \sim 113$ K), consistent with previous reports [10–12,15].

The critical strain of the magnetic transition observed via RXD coincides with the one determined from Raman spectroscopy, although it exhibits a broader profile due to spatial averaging over the larger x-ray beam footprint on the sample [18]. Together, these probes establish a strain-driven magnetic phase transition intrinsically linked to a massive modulation of the magnon gap.

RXD measurements also reveal a residual (1 0 2) reflection persisting up to the maximum applied strain ($\varepsilon \sim 0.22\%$), indicating the coexistence of a minority A-centered phase within the dominant B-centered phase. This observation is consistent with the post-transition Raman spectra [Fig. 1(e)]. Accordingly, we assign the dominant high-energy magnon peak to the B-centered majority and the minor, lower-energy peak to the residual A-centered phase, as supported by the close energy match between the latter and the pretransition magnon. Under further strain, the dominant magnon peak increases in intensity, while the weak one remains faint (Fig. S7 [18]).

Theory—To describe the strain dependence of the magnon gap, we employ an effective pseudospin model incorporating spin-orbit coupling (SOC) and crystal-field effects. The Ru^{4+} ion in Ca_2RuO_4 has a t_{2g}^4 configuration in a low-spin state with spin $s = 1$ and effective orbital moment $l = 1$; the SOC $\lambda \boldsymbol{s} \cdot \boldsymbol{l}$ entangles them into $\tilde{J} = 0$, 1 and 2 multiplets [24,34–36]. The $\tilde{J} = 0$ singlet forms the ground state, while the excited $\tilde{J} = 1$ triplet splits under a tetragonal field Δ into a $T_{x/y}$ doublet at energy E and a higher-energy

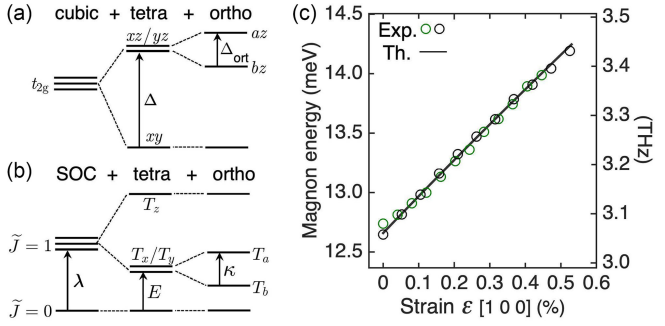


FIG. 3. (a) Splitting of $t_{2g}(xy, yz, xz)$ orbital states under tetragonal Δ and orthorhombic Δ_{ort} crystal fields. $\Delta > 0$ corresponds to flattened RuO_6 octahedra (xz/yz electron states above xy), while $\Delta_{\mathrm{ort}} > 0$ reflects a shorter a axis [$az = [1/\sqrt{2}](yz + xz)$ state above $bz = [1/\sqrt{2}](yz - xz)$]. (b) t_{2g}^4 energy levels including crystal-field and SOC effects (higher $\tilde{J} = 2$ states not shown). The ground-state singlet and the lowest doublet $T_{x/y}$ form an effective pseudospin $S = 1$ basis. (c) Experimental (circles) and theoretical (line) magnon energies under compressive strain along the [1 0 0] direction. Colors denote distinct datasets.

T_z level [Fig. 3(b)]. An orthorhombic field Δ_{ort} further splits the $T_{x/y}$ doublet into $T_{a/b}$ states by κ [Fig. 3(b)].

The energies E and κ, which quantify the lowest levels of the Ru^{4+} ions, are determined by λ and the crystal fields Δ and Δ_{ort}. We find that $E = \lambda(\frac{1}{2} + \sqrt{\frac{9}{4} - \delta + \delta^2} - \sqrt{1 + \delta^2})$, while the orthorhombic splitting κ, which governs the in-plane magnetic anisotropy, is given by

$$\kappa = \frac{1}{2}\left(1 - \frac{\delta}{\sqrt{1+\delta^2}}\right)\Delta_{\mathrm{ort}}, \tag{1}$$

where $\delta = (\Delta/2\lambda)$. In the strong SOC limit ($\Delta \ll \lambda$), the orbital moments remain unquenched ($\kappa \simeq \frac{1}{2}\Delta_{\mathrm{ort}}$); conversely, a large Δ induces orbital quenching, suppressing κ, which scales as $(\lambda/\Delta)^2\Delta_{\mathrm{ort}}$.

The level structure and excitations discussed above are mapped onto an effective $S = 1$ pseudospin basis comprising the $\tilde{J} = 0$ and $T_{a/b}$ states. Within this Hilbert space, the minimal Hamiltonian for quasi-two-dimensional Ca_2RuO_4 reads as [24]

$$\mathcal{H} = J\sum_{\langle ij\rangle}(\boldsymbol{S}_i \cdot \boldsymbol{S}_j - \tau S_{zi}S_{zj}) + E\sum_i S_{zi}^2 + \frac{1}{2}\kappa\sum_i (S_{ai}^2 - S_{bi}^2), \tag{2}$$

where $J > 0$ is the dominant in-plane nearest-neighbor exchange. The weak interlayer coupling $J_c \sim 10^{-2}$ meV [16,17] has a negligible contribution to the magnon spectra [24] and is thus omitted here. While the exchange anisotropy ($\tau > 0$) and single-ion anisotropy (E) confine the magnetic moments to the a-b plane, the orthorhombic term κ aligns them along the b axis [8,10,11,13,14] and opens an in-plane magnon gap:

$$\omega = \sqrt{\kappa[4J(2-\tau) + \frac{1}{2}\tau E + \kappa]}. \tag{3}$$

This expression highlights the strong sensitivity of the magnon gap (probed in the B_{1g} channel) to the anisotropy κ [Eq. (1)], which is highly tunable via the crystal fields and, thus, strain.

We first analyze the response of the magnon gap to compressive strain ε along the [1 0 0] direction, which enhances the lattice orthorhombicity [Fig. 1(b)]. This promotes the orbital splitting Δ_{ort}, thereby increasing κ [Eq. (1)]. Neglecting possible small variations of δ, we assume a linear relation $\kappa = \kappa_0(1 + \varepsilon/\varepsilon_0)$, where ε_0 is the intrinsic orthorhombicity and $\kappa_0 = g\varepsilon_0$ denotes the zero-strain anisotropy with pseudospin-lattice coupling strength g. Consequently, the strain-dependent magnon gap is obtained as

$$\omega \simeq \omega_0\sqrt{1 + \frac{\varepsilon}{\varepsilon_0}}, \tag{4}$$

where $\omega_0 = \sqrt{\kappa_0[4J(2-\tau) + \frac{1}{2}\tau E + \kappa_0]}$ is the intrinsic magnon gap.

Using the experimental values $\omega_0 = 12.7$ meV and $\varepsilon_0 = 2.2\%$, Eq. (4) provides an excellent fit to the [1 0 0] strain data [Fig. 3(c)]; see Supplemental Material [18] for the full set of modeling parameters. This consistency supports the linear relation between κ and ε, allowing us to extract $\kappa_0 \approx 3.6$ meV and $g = \kappa_0/\varepsilon_0 \approx 160$ meV.

In contrast to the previous case, compression along the [1 1 0] direction reduces the lattice orthorhombicity [Fig. 1(c)] and thus the orbital splitting Δ_{ort}. Assuming a linear decrease $\kappa = \kappa_0(1 - \varepsilon/\varepsilon_0)$ prior to the transition, we obtain a softened gap as follows:

$$\omega \simeq \omega_0\sqrt{1 - \frac{\varepsilon}{\varepsilon_0}}, \quad \text{when} \quad \varepsilon < \varepsilon_c. \tag{5}$$

With the same values for ω_0 and ε_0 quoted above, Eq. (5) agrees well with the experimental data below the critical strain $\varepsilon_c \sim 0.15\%$ [Fig. 4(a)]. At ε_c, the weak magnon peak associated with the residual A-centered phase exhibits a slight additional softening, attributed to a modest reduction in Δ_{ort} [Fig. S11(b) [18]].

Unexpectedly, the magnon energy in the B-centered phase exhibits an abrupt jump of ~1.3 meV at ε_c, despite strain along the [1 1 0] direction monotonically reducing the lattice orthorhombicity and the orbital splitting Δ_{ort}. This behavior stems from the dependence of κ [Eq. (1)] on the tetragonal field Δ: κ increases strongly as Δ decreases

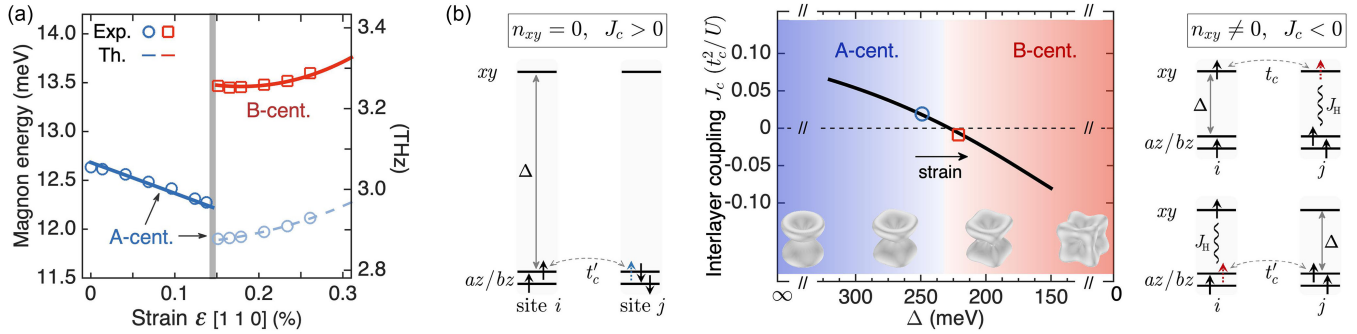


FIG. 4. (a) Measured magnon energies (circles and squares) and theoretical fits (lines, see details in Supplemental Material [18]) under compressive strain along the [1 1 0] direction. Blue and red denote A- and B-centered phases, respectively. Above $\varepsilon_c \sim 0.15\%$ (vertical line), light blue represents the residual A-centered phase. (b) Calculated interlayer coupling J_c (middle panel) as a function of tetragonal crystal field Δ. Compressive strain reduces Δ from 250 meV (blue circle) to 220 meV (red square) across ε_c, driving a sign change in J_c (from AFM to FM) that triggers the A-centered to B-centered transition. Bottom: visualization of t_{2g}^4 hole density at different Δ. At large Δ with suppressed xy-orbital hole density (left), interlayer hopping is restricted to channels favoring AFM coupling; at small Δ (right), the increased xy-orbital hole occupancy activates additional hopping paths that promote FM interactions via Hund's coupling J_H. Here, t_c (t_c') represents interlayer hopping between xy (az/bz) levels.

(Fig. S12 [18]), reflecting the enhancement of SOC effects toward the cubic limit with unquenched orbital moments. Quantitatively, a drop in Δ of ∼30 meV at ε_c, which enhances κ by ∼0.7 meV, can account for the observed ∼1.3 meV jump in the magnon gap [Fig. S11(b) [18]]. Such an abrupt change in the crystal fields across ε_c is intimately tied to structural modifications, consistent with the distinct change observed in the strain dependence of the phonon frequencies [Figs. 1(e) and S6(b) [18]].

Interestingly, as shown in Fig. 4(b), the strain-induced reduction of the tetragonal field Δ reverses the sign of the interlayer coupling J_c, thereby driving the transition from the A-centered to the B-centered magnetic structure. Microscopically, J_c is governed by the spin-orbital composition of the Ru electrons, which is determined by the interplay of crystal fields, SOC, and Hund's coupling (details are provided in Supplemental Material [18]). At large Δ, the ground state carries negligible xy-orbital hole density ($n_{xy} \sim 0$), and interlayer exchange is dominated by az/bz hopping, yielding an antiferromagnetic (AFM) $J_c > 0$ [left panel of Fig. 4(b)]. By contrast, a strain-reduced Δ increases the xy-orbital character of the spin-orbit entangled state. This activates xy-hopping channels that favor ferromagnetic (FM) interactions ($J_c < 0$) via Hund's coupling [right panel of Fig. 4(b)]. Thus, the strain-enhanced xy-orbital hole density (Fig. S14 [18]) flips the sign of J_c, ultimately driving the observed magnetic phase transition.

Discussion—The strain-stabilized B-centered phase emerges with reduced lattice orthorhombicity and an expanded c axis, consistent with earlier reports on doped and pressurized samples [8,10,11,13–15]. Notably, our approach triggers this magnetic transition with significantly smaller structural modifications (Table S2 [18]), highlighting the high efficiency of strain control over the magnetic states in Ca_2RuO_4.

By fine-tuning the Ca_2RuO_4 lattice via dilute substitution or epitaxial growth, the critical strain can be tuned close to zero. This would maximize the strain sensitivity of the magnon gap, analogous to superconducting transition-edge sensors for ultrasensitive cryogenic photon or particle detection [37]. In a THz magnon conduit, triggering this transition abruptly elevates the magnon energy, creating a potential barrier against magnons from strain-free regions and thus realizing an ultrasensitive magnonic switch. Furthermore, the extreme strain sensitivity near the phase transition should foster large nonlinearities as strain fields associated with a given magnon can affect the propagation of other magnons. Such nonlinearities may enable further transition-edge device functionalities.

In summary, our Letter reveals a pronounced modulation of the magnon gap across a strain-driven magnetic phase transition in Ca_2RuO_4, quantitatively explained by the *in situ* tuning of effective spin-orbit coupling on the Ru ions. The extreme sensitivity of both the magnetic ground state and the elementary excitations to strain offers tantalizing prospects for future ultrasensitive THz magnonic devices.

Acknowledgments—We acknowledge support from the European Research Council under Advanced Grant No. 101141844 (SpecTera). L. W. and S. H. are partially supported by the Alexander von Humboldt Foundation. H. L. acknowledges support from the National Natural Science Foundation of China under Grant No. 12574066 and the Fundamental Research Funds for the Central Universities under Grant No. KG202501. We thank DESY (Hamburg) for RXD beamtime at PETRA-III P09 (LTP II-20200008). We are grateful to J. Burkhardt, S. Mayer, H. Gretarsson, P. Wochner, B. Bruha, and J. Bertinshaw for

technical assistance and to C. Hicks and A. Mackenzie for the strain device and fruitful discussions.

Data availability—There are no publicly available research data or software supporting this manuscript. Requests for further information or data should be sent to the authors.

[1] B. Flebus *et al.*, The 2024 magnonics roadmap, J. Phys. Condens. Matter **36**, 363501 (2024).

[2] H.-H. Kim, K. Ueda, S. Nakata, P. Wochner, A. Mackenzie, C. Hicks, G. Khaliullin, H. Liu, B. Keimer, and M. Minola, Giant stress response of terahertz magnons in a spin-orbit Mott insulator, Nat. Commun. **13**, 6674 (2022).

[3] J. Cenker, S. Sivakumar, K. Xie, A. Miller, P. Thijssen, Z. Liu, A. Dismukes, J. Fonseca, E. Anderson, X. Zhu, X. Roy, D. Xiao, J.-H. Chu, T. Cao, and X. Xu, Reversible strain-induced magnetic phase transition in a van der Waals magnet, Nat. Nanotechnol. **17**, 256 (2022).

[4] D. Sun, D. A. Sokolov, R. Waite, S. Khim, P. Manuel, F. Orlandi, D. D. Khalyavin, A. P. Mackenzie, and C. W. Hicks, Heisenberg spins on an anisotropic triangular lattice: $PdCrO_2$ under uniaxial stress, New J. Phys. **23**, 123050 (2021).

[5] S. Shrestha, M. Krautloher, M. Zhu, J. Kim, J. Hwang, J. Kim, J.-W. Kim, B. Keimer, and A. Seo, Emergent interlayer magnetic order via strain-induced orthorhombic distortion in the 5*d* Mott insulator Sr_2IrO_4, Phys. Rev. B **105**, L100404 (2022).

[6] S. Pandey, H. Zhang, J. Yang, A. F. May, J. J. Sanchez, Z. Liu, J.-H. Chu, J.-W. Kim, P. J. Ryan, H. Zhou, and J. Liu, Controllable emergent spatial spin modulation in Sr_2IrO_4 by *in situ* shear strain, Phys. Rev. Lett. **129**, 027203 (2022).

[7] N. Stetzuhn, A. M. Kumar, S. Kovalchuk, D. Yagodkin, L. Simon, S. Mañas-Valero, E. Coronado, T. Taniguchi, K. Watanabe, D. Gill, S. Sharma, P. W. Brouwer, C. von Korff Schmising, S. Eisebitt, and K. I. Bolotin, Tunable magnons in a dual-gated 2D antiferromagnet, Nat. Commun. **17**, 5262 (2026).

[8] M. Braden, G. André, S. Nakatsuji, and Y. Maeno, Crystal and magnetic structure of Ca_2RuO_4: Magnetoelastic coupling and the metal-insulator transition, Phys. Rev. B **58**, 847 (1998).

[9] T. Takayama, J. Chaloupka, A. Smerald, G. Khaliullin, and H. Takagi, Spin-orbit-entangled electronic phases in 4*d* and 5*d* transition-metal compounds, J. Phys. Soc. Jpn. **90**, 062001 (2021).

[10] O. Friedt, M. Braden, G. André, P. Adelmann, S. Nakatsuji, and Y. Maeno, Structural and magnetic aspects of the metal-insulator transition in $Ca_{2-x}Sr_xRuO_4$, Phys. Rev. B **63**, 174432 (2001).

[11] P. Steffens, O. Friedt, P. Alireza, W. G. Marshall, W. Schmidt, F. Nakamura, S. Nakatsuji, Y. Maeno, R. Lengsdorf, M. M. Abd-Elmeguid, and M. Braden, High-pressure diffraction studies on Ca_2RuO_4, Phys. Rev. B **72**, 094104 (2005).

[12] H. Taniguchi, K. Nishimura, R. Ishikawa, S. Yonezawa, S. K. Goh, F. Nakamura, and Y. Maeno, Anisotropic uniaxial pressure response of the Mott insulator Ca_2RuO_4, Phys. Rev. B **88**, 205111 (2013).

[13] D. Pincini, S. Boseggia, R. Perry, M. J. Gutmann, S. Riccò, L. S. I. Veiga, C. D. Dashwood, S. P. Collins, G. Nisbet, A. Bombardi, D. G. Porter, F. Baumberger, A. T. Boothroyd, and D. F. McMorrow, Persistence of antiferromagnetic order upon La substitution in the $4d^4$ Mott insulator Ca_2RuO_4, Phys. Rev. B **98**, 014429 (2018).

[14] S. Chi, F. Ye, G. Cao, H. Cao, and J. A. Fernandez-Baca, Competition of three-dimensional magnetic phases in $Ca_2Ru_{1-x}Fe_xO_4$: A structural perspective, Phys. Rev. B **102**, 014452 (2020).

[15] D. G. Porter, F. Forte, V. Granata, M. Cannavacciuolo, R. Fittipaldi, M. Cuoco, A. Bombardi, and A. Vecchione, Guiding antiferromagnetic transitions in Ca_2RuO_4, Sci. Rep. **12**, 10957 (2022).

[16] H. Trepka, T. Keller, M. Krautloher, J. Xu, K. Habicht, M. Böhm, B. Keimer, and M. Hepting, Critical magnetic fluctuations in the layered ruthenates Ca_2RuO_4 and $Ca_3Ru_2O_7$, Phys. Rev. Res. **4**, 023181 (2022).

[17] S. Kunkemöller, D. Khomskii, P. Steffens, A. Piovano, A. A. Nugroho, and M. Braden, Highly anisotropic magnon dispersion in Ca_2RuO_4: Evidence for strong spin orbit coupling, Phys. Rev. Lett. **115**, 247201 (2015).

[18] See the Supplemental Material at http://link.aps.org/supplemental/10.1103/wk6v-1x5s for sample characterization, additional Raman and x-ray data, and details of the theoretical analysis, which includes Refs. [19,20].

[19] J. Zhang, A. S. McLeod, Q. Han, X. Chen, H. A. Bechtel, Z. Yao, S. N. Gilbert Corder, T. Ciavatti, T. H. Tao, M. Aronson, G. L. Carr, M. C. Martin, C. Sow, S. Yonezawa, F. Nakamura, I. Terasaki, D. N. Basov, A. J. Millis, Y. Maeno, and M. Liu, Nano-resolved current-induced insulator-metal transition in the Mott insulator Ca_2RuO_4, Phys. Rev. X **9**, 011032 (2019).

[20] D. B. Litvin, *Magnetic Group Tables* (International Union of Crystallography, Chester, United Kingdom, 2013).

[21] H.-H. Kim, S. M. Souliou, M. E. Barber, E. Lefrançois, M. Minola, M. Tortora, R. Heid, N. Nandi, R. A. Borzi, G. Garbarino, A. Bosak, J. Porras, T. Loew, M. König, P. J. W. Moll, A. P. Mackenzie, B. Keimer, C. W. Hicks, and M. Le Tacon, Uniaxial pressure control of competing orders in a high-temperature superconductor, Science **362**, 1040 (2018).

[22] H.-H. Kim, E. Lefrançois, K. Kummer, R. Fumagalli, N. B. Brookes, D. Betto, S. Nakata, M. Tortora, J. Porras, T. Loew, M. E. Barber, L. Braicovich, A. P. Mackenzie, C. W. Hicks, B. Keimer, M. Minola, and M. Le Tacon, Charge density waves in $YBa_2Cu_3O_{6.67}$ probed by resonant x-ray scattering under uniaxial compression, Phys. Rev. Lett. **126**, 037002 (2021).

[23] S.-M. Souliou, J. Chaloupka, G. Khaliullin, G. Ryu, A. Jain, B. J. Kim, M. Le Tacon, and B. Keimer, Raman scattering from Higgs mode oscillations in the two-dimensional antiferromagnet Ca_2RuO_4, Phys. Rev. Lett. **119**, 067201 (2017).

[24] A. Jain, M. Krautloher, J. Porras, G. H. Ryu, D. P. Chen, D. L. Abernathy, J. T. Park, A. Ivanov, J. Chaloupka, G. Khaliullin, B. Keimer, and B. J. Kim, Higgs mode and its

decay in a two-dimensional antiferromagnet, Nat. Phys. **13**, 633 (2017).

[25] H. Liu and G. Khaliullin, Pseudo-Jahn-Teller effect and magnetoelastic coupling in spin-orbit Mott insulators, Phys. Rev. Lett. **122**, 057203 (2019).

[26] S. Kunkemöller, E. Komleva, S. V. Streltsov, S. Hoffmann, D. I. Khomskii, P. Steffens, Y. Sidis, K. Schmalzl, and M. Braden, Magnon dispersion in $Ca_2Ru_{1-x}Ti_xO_4$: Impact of spin-orbit coupling and oxygen moments, Phys. Rev. B **95**, 214408 (2017).

[27] D. G. Porter, V. Granata, F. Forte, S. Di Matteo, M. Cuoco, R. Fittipaldi, A. Vecchione, and A. Bombardi, Magnetic anisotropy and orbital ordering in Ca_2RuO_4, Phys. Rev. B **98**, 125142 (2018).

[28] We also note that both phases have been proposed as altermagnets [29–31], with finite-momentum splitting between magnons of opposite chirality [32,33]. Such splitting is beyond our Raman measurements, which probe only zone-center magnons.

[29] G. Cuono, R. M. Sattigeri, J. Skolimowski, and C. Autieri, Orbital-selective altermagnetism and correlation-enhanced spin-splitting in strongly-correlated transition metal oxides, J. Magn. Magn. Mater. **586**, 171163 (2023).

[30] G. Cuono, F. Forte, A. Romano, and C. Noce, Emerging new phases in correlated Mott insulator Ca_2RuO_4, J. Phys. Condens. Matter **37**, 053002 (2025).

[31] A. Fakhredine, G. Cuono, J. Skolimowski, S. Picozzi, and C. Autieri, Interplay between relativistic spin-momentum locking and breaking of inversion symmetry: Conditions for effective p-wave magnetism, Mater. Horiz. **13**, 7108 (2026).

[32] L. Šmejkal, J. Sinova, and T. Jungwirth, Emerging research landscape of altermagnetism, Phys. Rev. X **12**, 040501 (2022).

[33] L. Šmejkal, A. Marmodoro, K.-H. Ahn, R. González-Hernández, I. Turek, S. Mankovsky, H. Ebert, S. W. D'Souza, O. Šipr, J. Sinova, and T. Jungwirth, Chiral magnons in altermagnetic RuO_2, Phys. Rev. Lett. **131**, 256703 (2023).

[34] G. Khaliullin, Excitonic magnetism in Van Vleck–type d^4 Mott insulators, Phys. Rev. Lett. **111**, 197201 (2013).

[35] H. Gretarsson, H. Suzuki, H. Kim, K. Ueda, M. Krautloher, B. J. Kim, H. Yavaş, G. Khaliullin, and B. Keimer, Observation of spin-orbit excitations and Hund's multiplets in Ca_2RuO_4, Phys. Rev. B **100**, 045123 (2019).

[36] C. G. Fatuzzo, M. Dantz, S. Fatale, P. Olalde-Velasco, N. E. Shaik, B. Dalla Piazza, S. Toth, J. Pelliciari, R. Fittipaldi, A. Vecchione, N. Kikugawa, J. S. Brooks, H. M. Rønnow, M. Grioni, C. Rüegg, T. Schmitt, and J. Chang, Spin-orbit-induced orbital excitations in Sr_2RuO_4 and Ca_2RuO_4: A resonant inelastic x-ray scattering study, Phys. Rev. B **91**, 155104 (2015).

[37] M. De Lucia, P. Dal Bo, E. Di Giorgi, T. Lari, C. Puglia, and F. Paolucci, Transition edge sensors: Physics and applications, Instruments **8**, 47 (2024).